A Bioinspired Elastic Hydrogel for Solar-Driven Water Purification

Xiaohui Xu, Sehmus Ozden, Navid Bizmark, Craig B. Arnold, Sujit S. Datta, and Rodney D. Priestley*

The global demand for clean and safe water will continue to grow well into the 21st century. Moving forward, the lack of access to clean water, which threatens human health and strains precious energy resources, will worsen as the climate changes. Therefore, future innovations that produce potable water from contaminated sources must be sustainable. Inspired by nature, a solar absorber gel (SAG) is developed to purify water from contaminated sources using only natural sunlight. The SAG is composed of an elastic thermoresponsive poly(*N*-isopropylacrylamide) (PNIPAm) hydrogel, a photo-thermal polydopamine (PDA) layer, and a sodium alginate (SA) network. Production of the SAG is facile; all processing is aqueous-based and occurs at room temperature. Remarkably, the SAG can purify water from various harmful reservoirs containing small molecules, oils, metals, and pathogens, using only sunlight. The SAG relies on solar energy to drive a hydrophilic/hydrophobic phase transformation at the lower critical solution temperature. Since the purification mechanism does not require water evaporation, an energy-intensive process, the passive solar water-purification rate is the highest reported. This discovery can be transformative in the sustainable production of clean water to improve the quality of human life.

1. Introduction

Providing reliable access to clean and safe water is a major global challenge in the 21st century.[1–3] Moreover, the demand for clean water will continue to increase due to the convergence of population growth, contamination of freshwater resources, and climate change.[4] According to a recent report published by the World Health Organization (WHO), more than 50% of the world's population will live in a water-stressed environment by 2025.[5] Such a future state-of-affairs will only exacerbate the public health crisis, including the current severe coronavirus disease 2019 (COVID-19) pandemic, related to disease transmission due to contaminated water or merely a lack of hand-washing stations. For instance, unsafe drinking water causes more than one-half million diarrheal deaths each year.[6] Medical expenses related to water-borne diseases, such as malaria, diarrhea, and worm infections may account for more than one-third of a household income in developing nations.[7] Therefore, addressing the water scarcity problem is of paramount importance to improve the quality of life and prosperity of society.

A solution to the water scarcity problem must be environmentally benign and not result in further strain on clean water availability. It is critical to avoid the crippling resource tradeoff between energy and water, that is, the so-called energy-water nexus. To that end, solar-driven water evaporation using sunlight is a promising sustainable strategy.[8–10] Tremendous effort has been dedicated to enhancing the rate of solar water purification, a key issue that must be addressed before adopting solar-driven water evaporation purification systems.[11–14] Nevertheless, due to the need to overcome the heat of vaporization, the water production rate via solar technologies remains insufficient to meet practical demands. Overcoming this barrier is critical for establishing solar purification as a future technology to improve clean water access.

The pufferfish, a fish species of the Tetraodontidae family, can inflate itself by intaking water when threatened and release it to return to its original shape when the threat of danger disappears; see **Figure 1**a. This absorption and release cycle of water by the pufferfish inspires our material's design approach. Specifically, poly(*N*-isopropyl acrylamide) (PNIPAm) hydrogels can absorb and release water via hydrophilic/hydrophobic switching at the lower critical solution temperature (LCST) (≈33 °C)—a temperature readily achieved using natural sunlight.[15,16] The application of thermally responsive hydrogels to regulate the transport of water has inherent attributes toward addressing water scarcity. As a practical manner, hydrogel-based systems

Dr. X. Xu, Dr. S. Ozden, Dr. N. Bizmark, Prof. S. S. Datta,
Prof. R. D. Priestley
Department of Chemical and Biological Engineering
Princeton University
Princeton, NJ 08544, USA
E-mail: rpriestl@princeton.edu
Dr. S. Ozden, Dr. N. Bizmark, Prof. C. B. Arnold, Prof. R. D. Priestley
Princeton Institute for the Science and Technology of Materials
Princeton University
Princeton, NJ 08544, USA
Prof. C. B. Arnold
Department of Mechanical and Aerospace Engineering
Princeton University
Princeton, NJ 08544, USA

**ADVANCED
SCIENCE NEWS**

www.advancedsciencenews.com
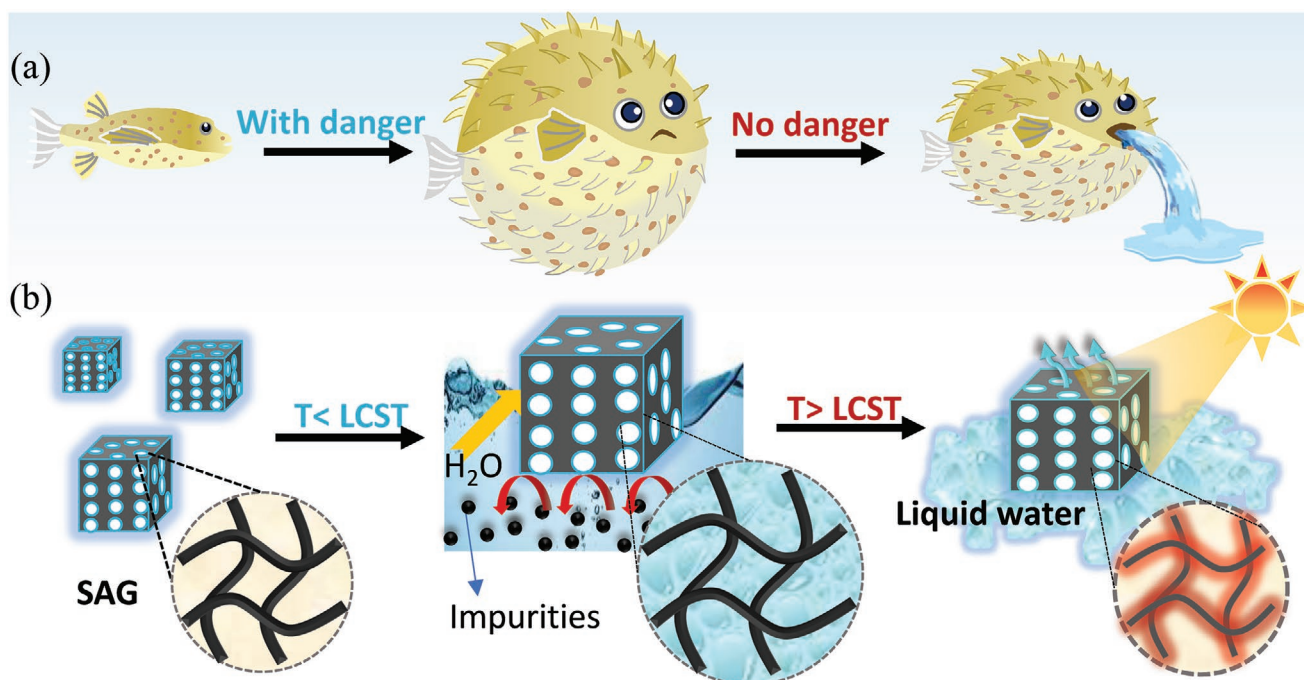
**ADVANCED
MATERIALS**

www.advmat.de

Figure 1. Sunlight-driven SAG technology for water production. a) The shape change of a pufferfish via the uptake and release of water when threatened. b) Inspired by the pufferfish, the SAG technology is based on the phase transformation (swelling and de-swelling) of PNIPAm under natural sunlight. SAG harvests large quantities of clean water from contaminated water at atmospheric temperature and generates clean water under natural sunlight.

are both scalable and modular. They also have a low environmental footprint and non-renewable energy requirements.[17] To enable hydrogels to harvest solar energy, they must be modified with an efficient solar absorber. Polydopamine (PDA), a melanin-based polymer that exhibits broadband solar absorption and noble photothermal conversion efficiency, can modify hydrogels.[18–20] Further, PDA offers additional properties of benefit for water purification: the presence of amino groups and aromatic rings endow PDA with the ability to remove heavy metal ions and organic dyes through chelation and hydrogen bonding.[21–24]

Inspired by the adsorption and release cycle of the pufferfish, we developed a photoresponsive solar absorber gel (SAG) with high elasticity to allow for repeated cycles of clean water production from harmful sources that is solely powered by natural sunlight, see Figure 1b. The SAG technology is fabricated by depositing PDA and cross-linked sodium alginate (SA) atop a macroporous PNIPAm hydrogel. The SA layer improves salt rejection of SAG.[25,26] The SAG technology operation is facile: upon immersion into contaminated water, SAG absorbs large quantities of clean water while salts, biologics, oils, and other pollutants are repelled. Once exposed to natural sunlight, solar absorption by the PDA thermally heats the SAG above the LCST of PNIPAm. Due to the hydrogel phase transformation from the swollen hydrophilic state to the collapsed hydrophobic state at the LCST, clean liquid water, as liquid and vapor, is expelled from SAG. This multi-modal mechanism of pure water production under natural sunlight opens a new paradigm for high-rate clean water production from contaminated water sources using renewable solar energy.

2. Results and Discussion

The SAG technology integrates the desired optical, thermal, elastic, and wetting properties into a single materials platform for solar-driven water purification: i) PNIPAm functions as the flexible water collection vessel and transport medium, ii) PDA functions as the broad spectrum light-to-thermal conversion material and pollutant filter, and iii) SA functions as the hydrophilic thermal insulator and a pollutant filter. The aqueous-based fabrication process of SAG is shown in **Figure 2**a. Traditional PNIPAm gel cross-linked with *N,N′*-methylene bisacrylamide (BIS) is brittle and not suitable for multi-cycle usage. Instead, SAG uses PNIPAm microgels as the crosslinker to improve elasticity and mechanical stability.[27] The PNIPAm was subsequently immersed into a dopamine tris-buffer solution (2 mg mL^{-1}) at room temperature to form a thin PDA layer atop the surface of the gel skeleton. The gel color turned black, confirming the successful coating (Figure S1, Supporting Information). Finally, cross-linked SA was adsorbed atop the PDA layer via coordination bonding between catechol groups of PDA and Cu^{2+} (see the Experimental Section for details).[28,29] SAG works by immersing it into a contaminated water source to absorb pure water while repelling harmful impurities. Subsequently, purified water is expelled from SAG when irradiated under one sun or exposed to natural sunlight. While capillary action drives water transport in SAG, the SA layer's filter efficiency significantly diminishes the possibility of fouling.

Figure 2 shows the structure of the gels. As revealed by SEM, the PNIPAm gel has a honeycomb-like structure with high porosity (Figure S2, Supporting Information), providing a good
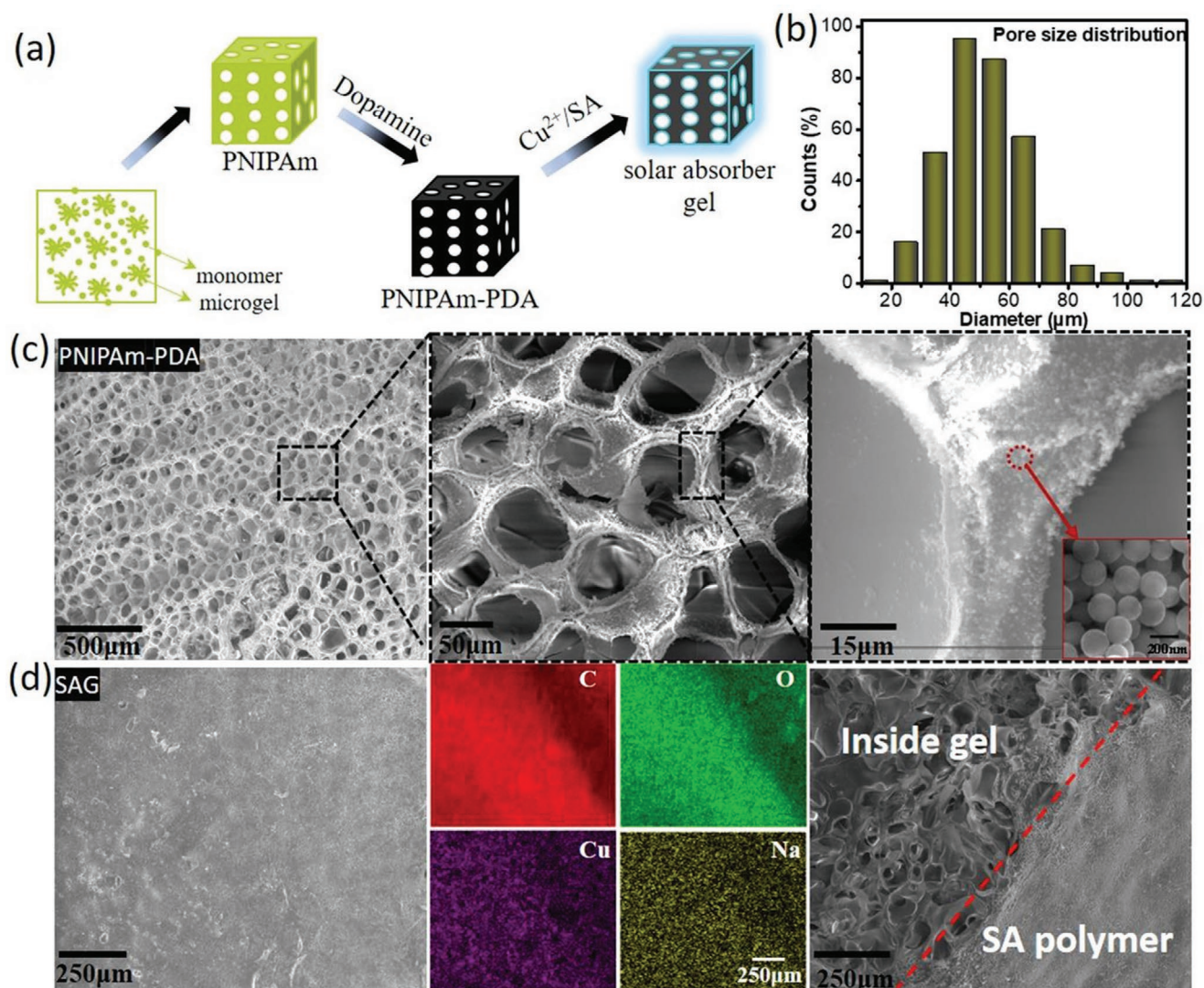
Figure 2. Preparation and morphology of SAG. a) Preparation of SAG at room temperature. b) Pore size distribution of PNIPAm–PDA hybrid gel. c) Scanning electron microscopy (SEM) images of the PDA decorated gel under different magnifications demonstrate macroporous architecture. d) SEM image; energy-dispersive X-ray spectroscopy of C, O, Cu, and Na elemental mapping images; and cross-sectional image of SAG.

structure for water transport via capillary flow. Following coating with the PDA, the hybrid gel preserved the interconnected porous structure with an average pore size of 50 μm (Figure 2b,c). Higher magnification revealed that PDA was indeed deposited atop the PNIPAm structure in the form of nanoparticles. Energy-dispersive X-ray (EDX) elemental mappings shows the existence of C K-edge, N K-edge, and O K-edge elements on PDA modified PNIPAm gel (Figure S3, Supporting Information). The SA coating led to a high density and homogenous polymer film atop the hydrogel surface (Figure 2d). The middle panel of Figure 2d shows EDX elemental mappings for Cu L-edge, C K-edge, Na K-edge, and O K-edge elements. Noticeably, both Cu and Na signals were uniformly distributed throughout the scanning area, and no N elements of PDA or PNIPAm were detected, further confirming the successful and well-controlled deposition of SA (with thickness of 1.2 μm, Figure S4, Supporting Information) atop the surface of the hybrid hydrogel.

A key requirement for reusable water decontamination is that SAG is elastic. Standard compression tests were conducted to demonstrate this property. As expected, the traditional, BIS-cross-linked PNIPAm gel was brittle and could not sustain compression. In contract, the microgel-cross-linked PNIPAm gel exhibited greater deformation under stress and complete recovery upon removal of the stress (Figure S5a,b and Movie S1, Supporting Information). After nine loading–unloading cycles at ≈80% strain, the modified PNIPAm gel maintained good mechanical stability (**Figure 3**a). The enhanced elasticity of the modified gel is due to its cross-linked microgel nanostructure. After functionalization with PDA and SA, the gel remained elastic. As shown in Figure 3a, the compressive stress–strain curve of SAG demonstrated that the recoverable compressive strain could reach 80%. The strain gradually decreased to zero as the stress was removed. Of note, SAG rapidly recovered its original shape after high compression
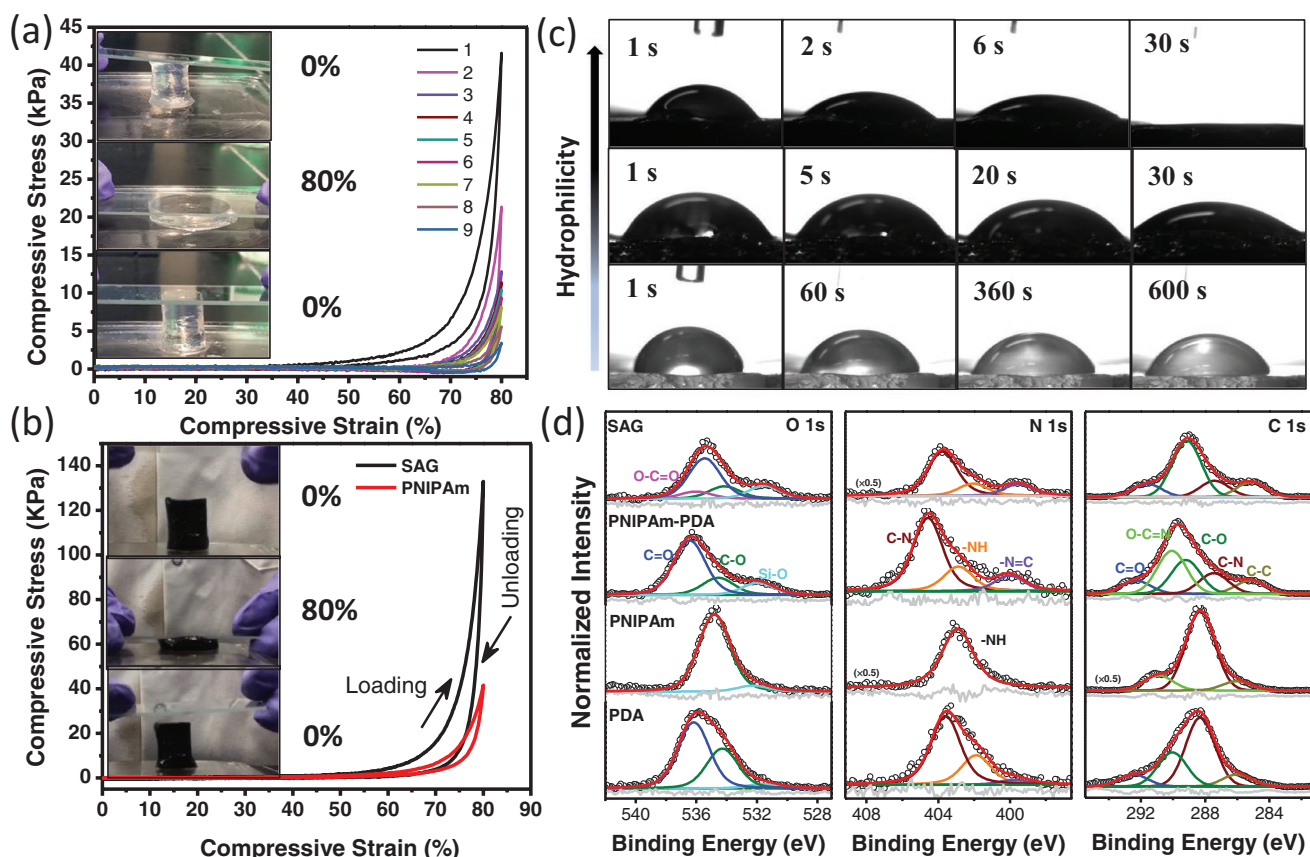
**ADVANCED
SCIENCE NEWS**

www.advancedsciencenews.com

**ADVANCED
MATERIALS**

www.advmat.de

Figure 3. Mechanical, wettability, and component characterization of SAG. a) The results of a nine-cycle fatigue test on the PNIPAm gel at a compressive strain of 80%. b) Reversible compressive stress–strain curves of SAG at a compressive strain of 80%; the insets are photographs of a compression–decompression test cycle. c) Optical images showing the dynamic wetting behaviors of a water droplet (≈30 µL) atop SAG (top), PDA-modified PNIPAm gel (middle), and PNIPAm gel (bottom) at room temperature. d) O 1s, N 1s, and C1s XPS spectra of the samples.

or extensive stretching (Figure S5c,d, Movie S2, Supporting Information).

The influence of PDA and SA on the wetting properties of PNIPAm was investigated by recording the dynamic wetting behavior of a water droplet at room temperature. As shown in Figure 3c, when placed atop PNIPAm, the water droplet remained stable with a water contact angle of ≈53°. In contrast, for the PDA-modified PNIPAm, the water contact angle decreased from ≈50° to ≈20° within 30 s due to polydopamine's hydrophilicity. Finally, the water droplet quickly imbibed into SAG, due to the combined SA and PDA layers, within 30 s. This indicates that SAG is hydrophilic, an essential requirement to facilitate water transport within the membrane and to reject hydrophobic contaminants, such as oil.

We also performed X-ray photoelectron spectroscopy (XPS) and Fourier transform infrared spectroscopy (FTIR) to confirm the chemical composition of SAG. From XPS of SAG (Figure S6a, Supporting Information), the peaks located at 530, 400, and 285 eV were assigned to oxygen (O), nitrogen (N), and carbon (C), and the peak appeared around 950 eV, corresponding to the binding energy of Cu^{2+}. Each element's high-resolution spectra provided further evidence for the successful modification of PNIPAm by PDA and SA (Figure 3d). From the FTIR spectra (Figure S6b, Supporting Information), a

broadband at ≈3400 cm^{-1} was attributed to the N–H stretching vibration of PNIPAm and the O–H stretching vibration of the hydroxyl groups on PDA. The peaks at 1643 cm^{-1} and 1551 cm^{-1} represent the typical C=O stretching and N–H stretching of PNIPAm, respectively.[30] Taken together, these results strongly indicate the formation of SAG, in good agreement with SEM characterizations.

Another merit of SAG is the rapid water release triggered by the phase transformation of PNIPAm at its LCST. The LCST was confirmed by differential scanning calorimetry (DSC) in **Figure 4a**. The LCST of PNIPAm was identified by the endothermic peak ≈34 °C and was unaffected by the treatment with PDA and SA.[31,32] The low-temperature LCST of SAG is critical to enable water purification under natural sunlight. Another essential requirement for solar-driven water production is broadband and efficient light absorption. The total solar absorbance of SAG was measured via UV–vis–NIR spectroscopy in the wavelength range of 200 to 1800 nm. As shown in Figure 4b, SAG exhibited broad and efficient absorption.

The low-temperature light-driven water release from SAG was assessed by simulated sunlight of 1 kW m^{-2} (1 sun). Under one sun illumination, the surface temperature of SAG increased with time and reached its LCST within 300 s of illumination (Figure 4c). The eventual surface temperature of SAG
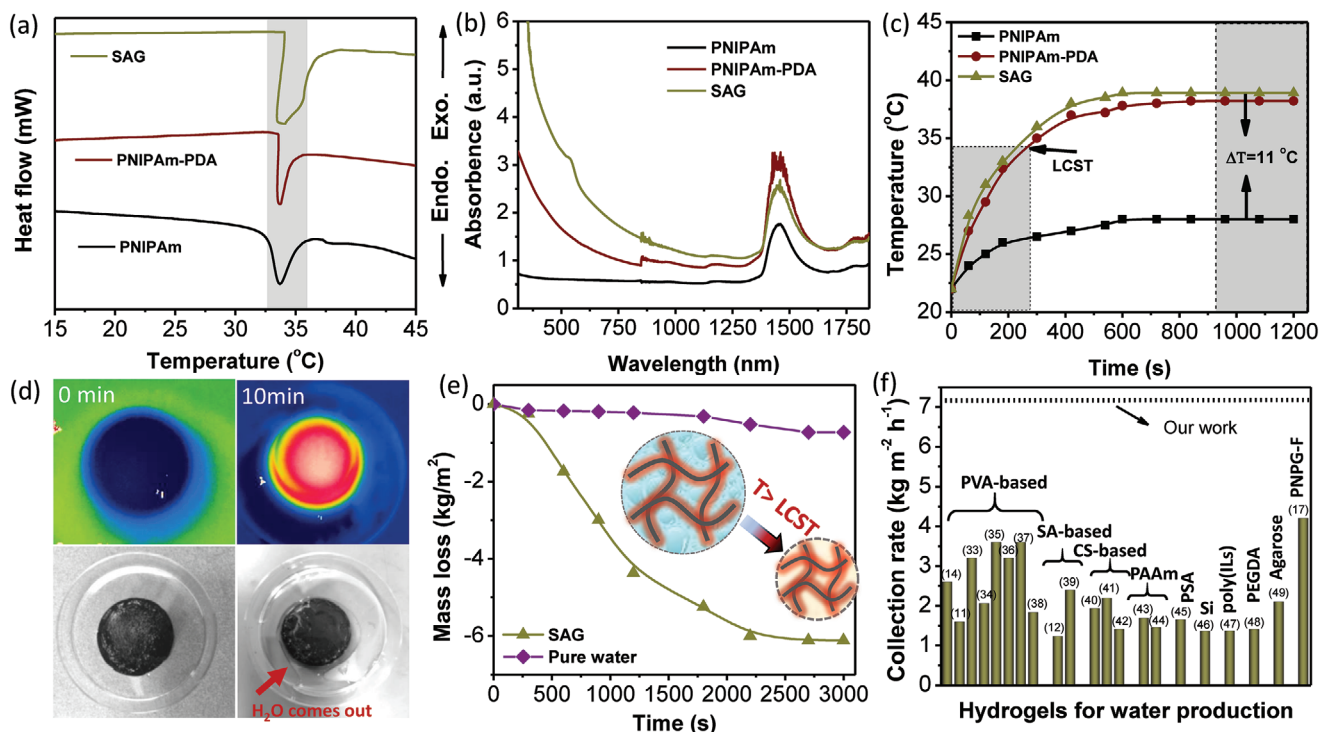
Figure 4. Light-trigged water release performance. a) DSC thermogram of swollen PNIPAm, PNIPAm–PDA, and SAG. b) UV–vis–NIR absorbance spectra of PNIPAm, PNIPAm–PDA, and SAG. c) Surface temperature change of various gels overtime under one sun illumination. d) IR images of the 3D porous gel under one sun irradiation. e) The mass change of pure water and water-swollen SAG under one sun irradiation. f) Comparison of water collection performance of SAG and the previously reported gels under one sun irradiation.

was ≈39 °C, ≈5 °C higher than the LCST. In contrast, irradiation raised the surface temperature of pure PNIPAm to ≈28 °C, well below the LCST. This comparison convincingly demonstrates the use of PDA as a photothermal conversation material. The PDA heating effect was also revealed by infrared images; see Figure S7, Supporting Information. The homogeneous distribution of hot areas again confirmed that PDA was uniformly distributed atop PNIPAm.

To test the water-swollen SAG water release rate, we performed a simple experiment by exposing it to simulated sunlight. At the LCST, the hydrophilicity of PNIPAm is switched via a conformational change. In response, any stored liquid water would be expelled. As shown in Figure 4d, exposure of SAG to simulated sunlight drove liquid water release. Also, minimal water vapor was collected by the evaporation–condensation process (Figure S7, Supporting Information). Therefore, SAG combines two water releasing modes into a single material platform. The SAG technology represents a clean water production mechanism unique beyond previously reported solar-driven water collection systems based solely on steam/vapor generation. In this regard, SAG overcomes the two major drawbacks associated with other solar-driven water collection systems' applicability: i) low water collection rate and ii) high energy requirement for evaporation.

As shown in Figure 4e, when water-swollen SAG was irradiated by one sun, the mass loss increased with time, and the weight change was ≈87.4% after 30 min, indicating that nearly all absorbed water within SAG was released. In comparison, pure water exhibited a negligible mass loss under the same

conditions. More remarkably, SAG's water collection rate reached 7.18 kg m^{-2} h^{-1} under one sun irradiation, see Figure 4f. Since the purification mechanism does not require water evaporation, an energy-intensive process, the water collection rate is higher than those that do rely on evaporation: poly(vinyl alcohol) (PVA),[11,14,33–38] alginate (SA),[12,39] chitosan (CS),[40–42] polyacrylamide (PAAm),[43,44] poly(sodium acrylate) (PSA),[45] silica gel,[46] poly(ionic liquid)s (PILs),[47] poly(ethylene glycol) diacrylate (PEGDA),[48] and agarose[49] (see Figure 4f). The high water collection rate of SAG is due to the thermoresponsive phase transformation of PNIPAm, which boosts the liquid water release at the LCST.

A sensible route to improving access to clean water is to obtain it from various contaminated sources after purification. SAG's water decontamination capability was tested in multiple model wastewater feedstocks containing small molecule dyes, heavy metals, oil, and yeast. First, three organic dyes (Rhodamine 6G (R6G), methyl orange (MO), and 4-nitrophenol (4-Nip)) with different sizes and surface charges (Figure S8, Supporting Information); and lead were selected as representative model contaminants to test solar-driven water of SAG. For R6G, the SAG rejected 97.1% and produced water with high purity, as evident by the color change, after one treatment cycle (**Figure 5**b). The SAG rejection rate of MO and 4-Nip samples was ≈87.7% and ≈84.0%, respectively, after one treatment cycle (Figure S9, Supporting Information). The high density of amine and catechol groups of PDA can strongly scavenge metals.[50] As shown in Figure 5c, after one treatment by SAG, the concentration of Pb^{2+} ions in contaminated water decreased
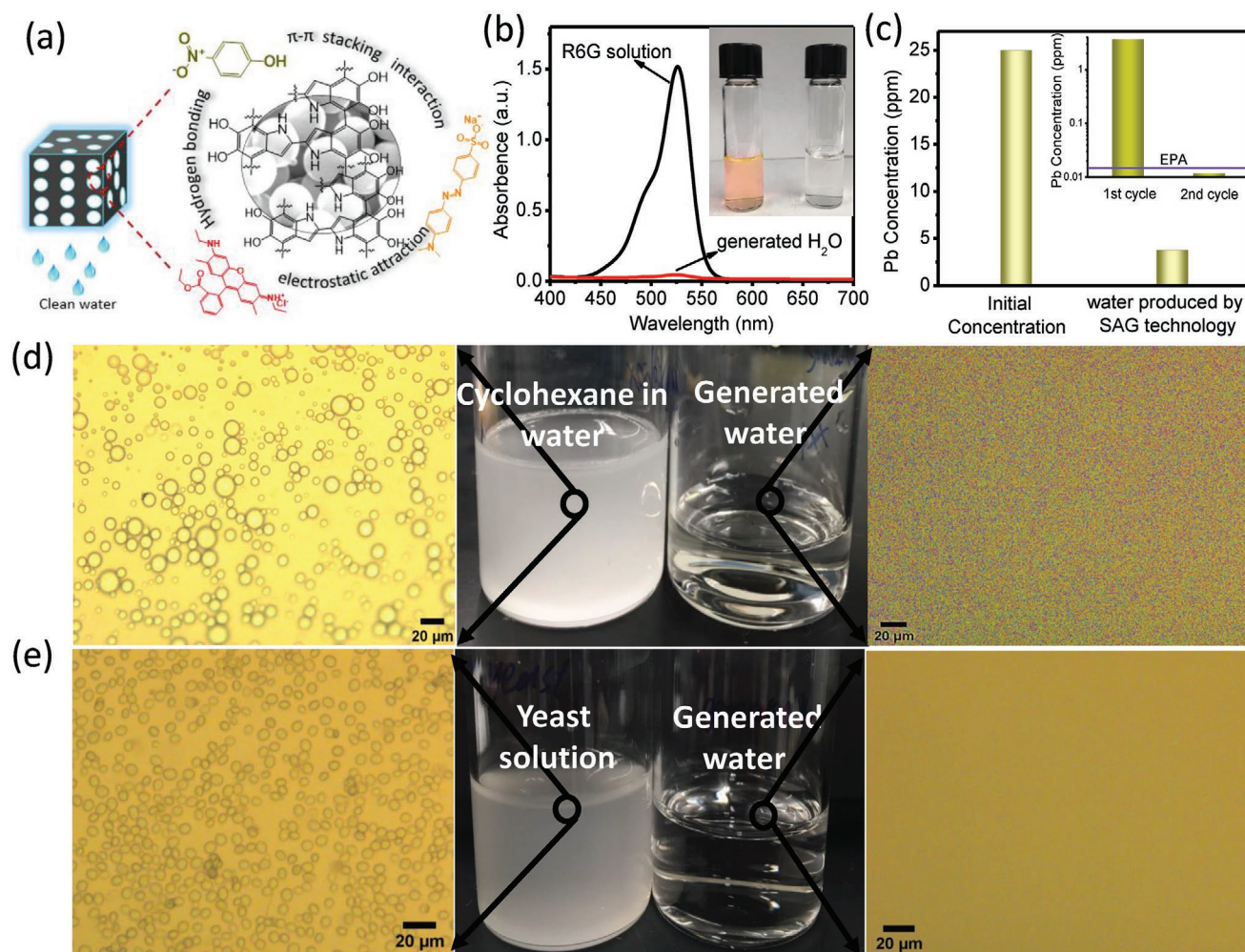
Figure 5. Evaluation of wastewater remediation. a) Schematic of clean water generation of SAG from dye contaminated water. b) UV–vis adsorption of simulated R6G-contaminated water and the generated water by SAG under one sun illumination. c) Concentration of Pb^{2+} in water purified by SAG. The inset image shows the changes of Pb^{2+} concentration after the second SAG treatment. d,e) Digital and microscopy photographs of SDS-stabilized cyclohexane-in-water emulsion (d) and yeast solution (e) before and after treatment with SAG.

25 to 3.7 ppm, making it a promising material to decontaminate heavy metal-containing water. In a second cycle, SAG reduced the Pb^{2+} concentrations from 3.7 to 0.012 ppm, which is below the US Environmental Protection Agency (EPA) allowable limits for drinking water. This impressive behavior is due to the introduction of PDA and SA into porous gel network. Another criterion for assessing the practicality of a wastewater purification material is its reusability. As shown in Figure S10, Supporting Information, SAG showed little deterioration of water purification after ten cycles. This is attributed to the SAG structure and adhesion between the different layers (Figure S11, Supporting Information).

Of practical importance is the purification of water from emulsified oil/water mixtures during cleanup and environmental remediation. SAG decontaminated water from three different emulsions comprising either hexane, cyclohexane, or petroleum ether. As shown in Figure 5d, the original cyclohexane-in-water emulsion was milky white, and the diameter of the cyclohexane droplets in the emulsion ranged from 1.0 to 20 μm (Figure S12a, Supporting Information).

After one SAG treatment, clean water was produced without evidence oil droplets (Figure 5d), as confirmed by DLS measurements (Figure S12b, Supporting Information). As for the other oil-in-water emulsions tested, SAG also generated purified water (Figure S13, Supporting Information). SAG's ability to create clean water from oil-in-water emulsions is attributed to the superhydrophilicity of SAG that prevents oil uptake.

The microbial level, especially harmful microbes, is a significant criterion for assessing water quality for human use. According to WHO, 80% of diseases are spread due to drinking unsafe water with bacteria contamination.[51] To test the rejection capability of microbes, SAG was placed into a 0.1wt% yeast solution. The microscopic images of the original yeast solution and the SAG-purified water are shown in Figure 5e. SAG produced clean water with no yeast cells, thus strongly indicating the possibility of potable water production for human consumption. The overall purification performance of SAG demonstrates its remarkable potential for diverse wastewater purification and microbe extraction.
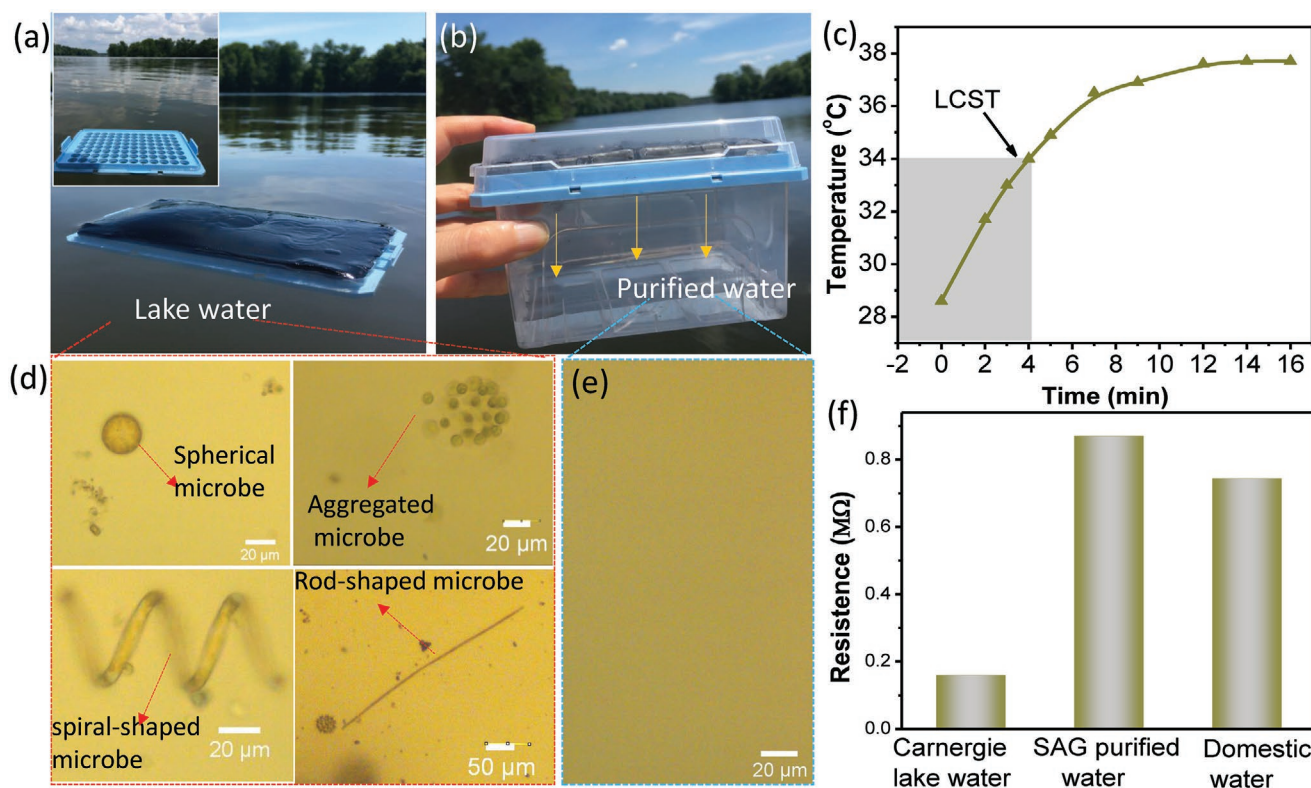
Figure 6. Natural sunlight-driven clean water generation. a,b) Photographs of the SAG purification system floating atop Carnegie Lake. b) Water-collection SAG system under natural sunlight. c) The surface temperature of SAG under natural sunlight. d,e) Optical images of Carnegie Lake water (d) and water purified by SAG (e). f) Conductivity of the Carnegie Lake water before and after SAG purification.

Alternative water resources, such as lake water, are a promising option to produce water safe for human consumption. We applied SAG to transform water from Carnegie Lake (Princeton, NJ, USA) into potable water. A water purification system fabricated from SAG with a cuboid structure (11 cm × 7.0 cm × 1.0 cm) atop a porous plate was floated atop Carnegie Lake (Figure S14, Supporting Information). As the lake surface temperature was ≈25 °C, SAG absorbed water (**Figure 6**a). Subsequently, clean water was generated by the purification system under natural sunlight (Figure 6b). As shown in Figure 6c, the surface temperature of SAG increased to ≈38 °C, convincingly demonstrating the capability of SAG to convert natural sunlight into thermal energy. The absorbed water was released from SAG and flowed to the container's bottom through the porous plate (Movie S3, Supporting Information). The microscopy images of water from Carnegie Lake before and after treatment revealed that various microbes were removed to produce potable water (Figure 6d,e; and Figure S15, Supporting Information). The purified water quality was further compared to domestic water by measuring the resistivity (Figure 6f). The resistance values of water from Carnegie Lake, SAG-purified water from Carnegie Lake, and domestic water were 0.16, 0.87, and 0.74 MΩ, respectively (Figure 6f; and Figure S16, Supporting Information), indicating effective purification. Finally, we remark that the purified water temperature was ≈30 °C, showing the main mechanism of water purification is by a phase transformation (Figure S17, Supporting Information) and not water evaporation. SAG is a

cost-effective technology to produce potable water from many non-potable water feedstocks. Further, our outdoor experiments reveal that SAG is energy efficient and operates under natural sunlight, demonstrating its practical applications in the future sustainable clean water generation.

3. Conclusion

With a water purification rate of 7.18 kg m^{-2} h^{-1} under sunlight, the development of SAG should be of interest to both industry and governments that are concerned with improving access to clean water in a sustainable, low-energy approach to the world's population. The technology is both scalable and modular and may be used to purify water from various sources. It is our desire that these attractive features may pave the way for SAG to improve the health of many in society by providing access to a vital resource, clean water.

4. Experimental Section

Materials: Dopamine hydrochloride, tris-base, *N*-isopropylacrylamide (NIPAm), *N,N'*-methylenebisacrylamide (Bis), potassium persulfate (KPS, K$_2$S$_2$O$_8$), *N,N,N',N'*-tetramethyl-ethylenediamine (TEMED), sodium dodecyl sulfate (SDS), copper(II) chloride (CuCl$_2$), and sodium alginate (SA) were commercially available from Sigma–Aldrich and used without further purification.

Preparation of 3D Solar Absorber Gels: The preparation of the hybrid gel followed a previously reported procedure to improve mechanical properties.[27] Specifically, 4.8 mg of KPS initiator was mixed with 4 mL of aqueous solution containing 90 mg of NIPAm monomer, 5 mg Bis and 21.6 mg SDS at 65 °C for 40 min under magnetic stirring. The PNIPAm microgels were formed until the transparent solution changed to opaque (FigureS18, Supporting Information). Next, the opaque mixture was put in an ice-water bath, and 0.56 g of NIPAm was added in the reaction, followed by addition of 40 μL of TEMED accelerator. The above mixture was sealed at 5 °C overnight, forming a transparent PNIPAm gel (i.e., microgel-cross-linked PNIPAm gel). To compare the mechanical properties, a traditional PNIPAm gel was prepared via polymerization of NIPAm at room temperature without the addition of SDS. For the dopamine functionalization step, 1 M tris-HCl buffer solution was first prepared by dissolving 12.1 g of tris-base and 3 mL HCl in 100 mL of water. The obtained PNIPAm gel was immersed into 50 mL of 10 mM tris-HCl buffer solution before adding dopamine hydrochloride (100 mg). After 12 h, the PNIPAm gel was taken out and put into fresh dopamine tris-buffer solution (50 mL, 2 mg mL^{-1}) under stirring for 12 h until a dark gel was formed. Then, the as-prepared product was immersed in a 0.1 M CuCl$_2$ solution and a 0.1 wt% sodium alginate solution to obtain the SAG gels.[28] In the SAG, the mass percentage of PDA, PNIPAm, and SA was 19%, 66%, and 14% respectively.

LCST Determination: The LCST of gels were determined by differential scanning calorimeter (DSC-8500). Before each measurement, all samples were put in distilled water to reach the equilibrium state, and excess water on the surface was removed using filter paper. Samples (≈30 mg) were then loaded in aluminum cells and sealed hermetically. The thermal analysis was performed in a temperature range of 15–45 °C with a heating rate of 0.5 °C min^{-1} in a dry N$_2$ atmosphere (with a flow rate of 50 mL min^{-1}).

Calculation of Water Collection Efficiency: To measure the water collection efficiency, the swollen 3D porous gels were exposed to simulated sunlight with a radiation intensity of 1 kW m^{-2} (one sun, 300 W xenon arc lamp) in air at an ambient temperature of 20 °C. Temperature variation of the 3D porous gels was measured by using a thermometer at each time interval. Simultaneously, distilled water served as a blank control and its temperature was evaluated at the same condition. The mass change of SAG was recorded by an electronic mass balance at various times. Because of the hydrophilicity switching of PNIPAm and heating effect of polydopamine, the weight loss over the entire process was due to water release.

Water Collection from Contaminated Water: To test water purification capability of SAG from polluted water, oil-, dye-, and microbe-contaminated water were selected as models. To prepare oil wastewater models, hexane, cyclohexane, and petroleum ester-in-water emulsions, were mixed, respectively, with a 0.5 mg L^{-1} SDS water solution in a mass ratio of 1:99 and then mixed at 1000 rpm for 30 min. The clean water collection process was carried out by immersing SAG in the prepared mixture for 3 h, and then the swollen SAG was taken out and irradiated with sunlight to generate clean water.

Materials Characterization: The morphologies and elemental mapping of the as-prepared gels were characterized by an environmental scanning electron microscope (Quanta 200 FE-ESEM). FTIR spectra of dried samples were obtained using a Thermo FTIR Imaging Microscope (Nicolet iN10 MX). Water contact angle was measured on an OCA20 machine (Data-physics). The temperature distribution was recorded using an IR camera (FLIR Thermal Camera) in real-time and the temperature of the top surface of the gels were tested using a thermometer (Omega HH74K). The absorptance spectra of the wet samples were measured on a UV–vis–NIR spectrometer (Agilent Technologies, Cary 5000). The X-ray diffraction (XRD) patterns were recorded using a high-resolution X-ray diffractometer (Bruker D8 Discover). X-ray photoelectron spectroscopy (XPS) analyses were performed using an X-ray photoelectron spectrometer (Thermo K-alpha XPS/UPS).

Supporting Information

Supporting Information is available from the Wiley Online Library or from the author.

Conflict of Interest

The authors declare no conflict of interest.

Author Contributions

R.D.P. coordinated the project; X.X. synthesized materials and conducted characterization with aid from S.O. and N.B; all authors discussed and interpreted the results, and contributed to writing the manuscript.

Data Availability Statement

The data that support the findings of this study are available from the corresponding author upon reasonable request.

[1] C. J. Vörösmarty, P. Green, J. Salisbury, R. B. Lammers, *Science* **2000**, *289*, 284.

[2] M. A. Shannon, P. W. Bohn, M. Elimelech, J. G. Georgiadis, B. J. Marinas, A. M. Mayes, *Nanoscience and Technology: A Collection of Reviews from Nature Journals*, World Scientific, Singapore **2010**, p. 337.

[3] C. J. Vörösmarty, P. B. Mcintyre, M. O. Gessner, D. Dudgeon, A. Prusevich, P. Green, S. Glidden, S. E. Bunn, C. A. Sullivan, C. R. Liermann, *Nature* **2010**, *467*, 555.

[4] A. E. Ercin, A. Y. Hoekstra, *Environ. Int.* **2014**, *64*, 71.

[5] *WHO/UNICEF Joint Monitoring Programme for Water Supply and Sanitation. Progress on drinking water and sanitation: 2014 update*, WHO Press, Geneva, Switzerland **2014**.

[6] *Preventing Diarrhoea through Better Water, Sanitation and Hygiene: Exposures and Impacts in Low-and Middle-Income Countries*, World Health Organization, Geneva, Switzerland **2014**.

[7] A. Malik, A. Yasar, A. Tabinda, M. Abubakar, *Iran. J. Public Health* **2012**, *41*, 39.

[8] H. Ghasemi, G. Ni, A. M. Marconnet, J. Loomis, S. Yerci, N. Miljkovic, G. Chen, *Nat. Commun.* **2014**, *5*, 4449.

[9] S. He, C. Chen, Y. Kuang, R. Mi, Y. Liu, Y. Pei, W. Kong, W. Gan, H. Xie, E. Hitz, *Energy Environ. Sci.* **2019**, *12*, 1558.

[10] P. Mu, Z. Zhang, W. Bai, J. He, H. Sun, Z. Zhu, W. Liang, A. Li, *Adv. Energy Mater.* **2019**, *9*, 1802158.

[11] F. Yu, X. Ming, Y. Xu, Z. Chen, D. Meng, H. Cheng, Z. Shi, P. Shen, X. Wang, *Adv. Mater. Interfaces* **2019**, *6*, 1901168.

[12] X. Zhao, C. Liu, *Desalination* **2020**, *482*, 114385.

[13] K. Yu, P. Shao, P. Meng, T. Chen, J. Lei, X. Yu, R. He, F. Yang, W. Zhu, T. Duan, *J. Hazard. Mater.* **2020**, *392*, 122350.

[14] Y. Guo, F. Zhao, X. Zhou, Z. Chen, G. Yu, *Nano Lett.* **2019**, *19*, 2530.

[15] R. Ou, J. Wei, L. Jiang, G. P. Simon, H. Wang, *Environ. Sci. Technol.* **2016**, *50*, 906.

[16] S. Huang, X. Liu, Q. Hu, T. Wei, J. Wang, H. Chen, C. Wu, *ACS Appl. Mater. Interfaces* **2020**, *12*, 2991.

[17] H. Geng, Q. Xu, M. Wu, H. Ma, P. Zhang, T. Gao, L. Qu, T. Ma, C. Li, *Nat. Commun.* **2019**, *10*, 1512.

[18] B. Poinard, S. Z. Y. Neo, E. L. L. Yeo, H. P. S. Heng, K. G. Neoh, J. C. Y. Kah, *ACS Appl. Mater. Interfaces* **2018**, *10*, 21125.

[19] Q. Jiang, H. G. Derami, D. Ghim, S. Cao, Y.-S. Jun, S. Singamaneni, *J. Mater. Chem. A* **2017**, *5*, 18397.

[20] Y. Zhang, X. Yin, B. Yu, X. Wang, Q. Guo, J. Yang, *ACS Appl. Mater. Interfaces* **2019**, *11*, 32559.

[21] K. Cui, B. Yan, Y. Xie, H. Qian, X. Wang, Q. Huang, Y. He, S. Jin, H. Zeng, *J. Hazard. Mater.* **2018**, *350*, 66.

[22] W.-X. Mao, X.-J. Lin, W. Zhang, Z.-X. Chi, R.-W. Lyu, A.-M. Cao, L.-J. Wan, *Chem. Commun.* **2016**, *52*, 7122.

[23] W. Weng, C. Zeng, W. Xiao, *J. Hazard. Mater.* **2019**, *11*, 9156.

[24] P. A. RüHs, K. G. Malollari, M. R. Binelli, R. Crockett, D. W. Balkenende, A. R. Studart, P. B. Messersmith, *ACS Nano* **2020**, *14*, 3885.

[25] C. Yu, Y. Wang, X. Lang, S. Fan, *Environ. Sci. Technol.* **2016**, *50*, 13024.

[26] W. Hu, L. Xie, H. Zeng, *J. Colloid Interface Sci.* **2020**, *568*, 36.

[27] L.-W. Xia, R. Xie, X.-J. Ju, W. Wang, Q. Chen, L.-Y. Chu, *Nat. Commun.* **2013**, *4*, 2226.

[28] S. J. Gao, Y. Z. Zhu, J. L. Wang, F. Zhang, J. Y. Li, J. Jin, *Adv. Funct. Mater.* **2018**, *28*, 1801944.

[29] R. Ge, M. Lin, X. Li, S. Liu, W. Wang, S. Li, X. Zhang, Y. Liu, L. Liu, F. Shi, *ACS Appl. Mater. Interfaces* **2017**, *9*, 19706.

[30] X. Xu, B. Bai, H. Wang, Y. Suo, *ACS Appl. Mater. Interfaces* **2017**, *9*, 6424.

[31] S. Pfensig, D. Arbeiter, K.-P. Schmitz, N. Grabow, T. Eickner, S. Illner, *Curr. Dir. Biomed. Eng.* **2016**, *2*, 1

[32] C. H. Zhu, Y. Lu, J. F. Chen, S. H. Yu, *Small* **2014**, *10*, 2796.

[33] F. Zhao, X. Zhou, Y. Shi, X. Qian, M. Alexander, X. Zhao, S. Mendez, R. Yang, L. Qu, G. Yu, *Nat. Nanotechnol.* **2018**, *13*, 489.

[34] G. Hu, Y. Cao, M. Huang, Q. Wu, K. Zhang, X. Lai, J. Tu, C. Tian, J. Liu, W. Huang, *Energy Technol.* **2020**, *8*, 1900721.

[35] Y. Guo, X. Zhou, F. Zhao, J. Bae, B. Rosenberger, G. Yu, *ACS Nano* **2019**, *13*, 7913.

[36] Y. Guo, H. Lu, F. Zhao, X. Zhou, W. Shi, G. Yu, *Adv. Mater.* **2020**, *32*, 1907061.

[37] X. Zhou, F. Zhao, Y. Guo, B. Rosenberger, G. Yu, *Sci. Adv.* **2019**, *5*, eaaw5484.

[38] M. Tan, J. Wang, W. Song, J. Fang, X. Zhang, *J. Mater. Chem. A* **2019**, *7*, 1244.

[39] Z. Guo, F. Yu, Z. Chen, Z. Shi, J. Wang, X. Wang, *Sol. Energy Mater. Sol. Cells* **2020**, *211*, 110531.

[40] W. Wang, J. Niu, J. Guo, L. Yin, H. Huang, *Sol. Energy Mater. Sol. Cells* **2019**, *201*, 110046.

[41] F. Yu, Z. Chen, Z. Guo, M. S. Irshad, L. Yu, J. Qian, T. Mei, X. Wang, *ACS Sustainable Chem. Eng.* **2020**, *8*, 7139.

[42] S. Singh, N. Shauloff, R. Jelinek, *ACS Sustainable Chem. Eng.* **2019**, *7*, 13186.

[43] X. Liang, X. Zhang, Z. Liu, Q. Huang, H. Zhang, C. Liu, Y. Liu, *Sol. Energy* **2020**, *201*, 581.

[44] L. Zhao, P. Wang, J. Tian, J. Wang, L. Li, L. Xu, Y. Wang, X. Fei, Y. Li, *Sci. Total Environ.* **2019**, *668*, 153.

[45] J. Zeng, Q. Wang, Y. Shi, P. Liu, R. Chen, *Adv. Energy Mater.* **2019**, *9*, 1900552.

[46] M. Gao, C. K. Peh, H. T. Phan, L. Zhu, G. W. Ho, *Adv. Energy Mater.* **2018**, *8*, 1870114.

[47] C. Xiao, W. Liang, Q.-M. Hasi, L. Chen, J. He, F. Liu, C. Wang, H. Sun, Z. Zhu, A. Li, *Mater. Today Energy* **2020**, *16*, 100417.

[48] X. Yin, Y. Zhang, Q. Guo, X. Cai, J. Xiao, Z. Ding, J. Yang, *ACS Appl. Mater. Interfaces* **2018**, *10*, 10998.

[49] Z. Sun, J. Wang, Q. Wu, Z. Wang, Z. Wang, J. Sun, C. J. Liu, *Adv. Funct. Mater.* **2019**, *29*, 1901312.

[50] D. T. Sun, L. Peng, W. S. Reeder, S. M. Moosavi, D. Tiana, D. K. Britt, E. Oveisi, W. L. Queen, *ACS Cent. Sci.* **2018**, *4*, 349.

[51] L. Liu, H. L. Johnson, S. Cousens, J. Perin, S. Scott, J. E. Lawn, I. Rudan, H. Campbell, R. Cibulskis, M. Li, *Lancet* **2012**, *379*, 2151.